Chemosphere 202 (2018) 686–693

Contents lists available at ScienceDirect

Chemosphere

journal homepage: www.elsevier.com/locate/chemosphere

From biowaste to magnet-responsive materials for water remediation from polycyclic aromatic hydrocarbons

Roberto Nisticò [a, b, 1], Federico Cesano [a, c, 1], Flavia Franzoso [a], Giuliana Magnacca [a, c], Domenica Scarano [a, c], Israel G. Funes [d], Luciano Carlos [e], Maria E. Parolo [d, *]

[a] University of Torino, Department of Chemistry, Via P. Giuria 7, 10125 Torino, Italy
[b] Polytechnic of Torino, Department of Applied Science and Technology DISAT, C.so Duca degli Abruzzi 24, 10129 Torino, Italy
[c] NIS Interdepartment Centre, Via P. Giuria 7, 10125 Torino, Italy
[d] Instituto de Investigación en Toxicología Ambiental y Agrobiotecnología, CITAAC (CONICET-UNCo), Facultad de Ingeniería, Universidad Nacional Del Comahue, Buenos Aires 1400, 8300 Neuquén, Argentina
[e] Instituto de Investigación y Desarrollo en Ingeniería de Procesos, Biotecnología y Energías Alternativas, PROBIEN (CONICET-UNCo), Facultad de Ingeniería, Universidad Nacional Del Comahue, Buenos Aires 1400, 8300 Neuquén, Argentina

HIGHLIGHTS

- Biowaste-derived substances coated iron oxides are successfully used for PAHs removal.
- Thermally treated NPs show high adsorption capacity for PAHs.
- The reusability of NPs after six cycles is found to be excellent.
- Results encouraged the application of these NPs in wastewater remediation.

GRAPHICAL ABSTRACT

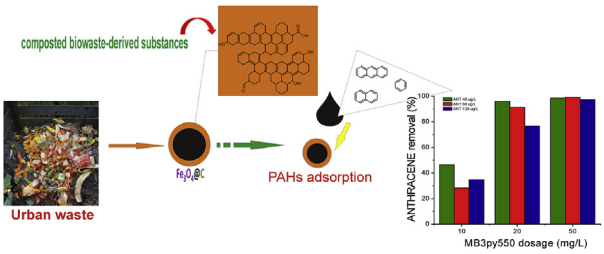

ARTICLE INFO

Article history:
Received 25 January 2018
Received in revised form
21 March 2018
Accepted 22 March 2018
Available online 23 March 2018

Handling Editor: Y Yeomin Yoon

Keywords:
Adsorption
Biomass valorization
Iron oxides
Magnetic nanomaterials
Pyrolysis

ABSTRACT

Composted urban biowaste-derived substances (BBS-GC) are used as carbon sources for the preparation of carbon-coated magnet-sensitive nanoparticles obtained via co-precipitation method and the subsequent thermal treatment at 550 °C under nitrogen atmosphere. A multitechnique approach has been applied to investigate the morphology, magnetic properties, phase composition, thermal stability of the obtained magnet-sensitive materials. In particular, pyrolysis-induced modifications affecting the BBS-GC/carbon shell were highlighted. The adsorption capacity of such bio-derivative magnetic materials for the removal of hydrophobic contaminants such as polycyclic aromatic hydrocarbons was evaluated in order to verify their potential application in wastewater remediation process. The promising results suggest their use as a new generation of magnet-responsive easily-recoverable adsorbents for water purification treatments.

1. Introduction

In recent years, a wide number of studies has been dedicated to the valorization of biowaste and biowaste-derived substances in order to prepare novel smart products, thus reaching a reduction of

* Corresponding author.
E-mail addresses: maria.parolo@fain.uncoma.edu.ar, meparolo@gmail.com (M.E. Parolo).
[1] Both authors contributed equally to this work.

https://doi.org/10.1016/j.chemosphere.2018.03.153
0045-6535/

the industrial and/or urban residues, re-entering them in the economic cycle in a more sustainable and environmental-friendly development of our society (Fava et al., 2015; G. Magnacca et al., 2015; Deng et al., 2016; Nisticò, 2017a). In particular, low-cost starting materials from natural sources (i.e., clays and minerals as well as biopolymers), industrial wastes and agriculture residues (such as lignin and humic/fulvic acid-like substances, chitin and chitosan, alginate and waste slurry), are considered as an important source of fine chemicals in substitution of the more traditional petroleum-derived ones (Bailey et al., 1999; Avetta et al., 2014; Vakili et al., 2014; Bautista et al., 2015; Choi et al., 2015a, 2015b; Manna et al., 2015; Nisticò et al., 2015; Franzoso et al., 2016). Among these low-cost bio-based sources, lignocellulose-derived materials and chitin/chitosan seem to be highly attractive resources for the future generation of chemicals (Tran et al., 2015).

Shape- and size-controlled smart magnetic nanoparticles (mNPs) consisting in a magnet-sensitive core made of iron oxides (i.e., magnetite/maghemite) stabilized by one or more covering layer(s), currently attracted the interests of worldwide experts due to their unique magnet-responsive properties which favor their uses in several technological applications, such as drug-delivery or contaminated wastewater (bio)remediation processes (Cesano et al., 2016; Lata and Samadder, 2016; Zhao et al., 2016; Lu et al., 2007; Nisticò, 2017b). In this context, various protective and/or stabilizing materials were investigated for inducing particular surface properties at the mNPs. Typically, both oxides (mainly silica) and/or organic (surfactants, (bio)polymers, and carbons) coatings were considered as possible covering-materials, thus combining the advantages of both components selected (namely, the magnet-sensitive Fe-containing oxides core and the functionality at the surface) (Lu et al., 2007; Li et al., 2013; Nardi et al., 2013).

As already evidenced in our previous works (Nisticò et al., 2015, 2018; Franzoso et al., 2017), Bio-Based Substances (BBS-GC, where GC stands for green compost) are supramolecular aggregates made of organic macromolecules with a highly branched and complex lignin-derived structure. Such substances are isolated from urban composted biowastes after more than 180 days of composting, and as a consequence of the starting material complexity (i.e., urban public park trimming and home gardening residues), BBS-GC contain several functional groups (the BBS-GC chemical structure and functionalities are fully reported in Table S1, whereas their thermal stability is reported in Fig. S1) (Nisticò et al., 2015). The macromolecular nature of these BBS, very similar to humic/fulvic substances with several O-containing functional groups, suggested their potential use as stabilizing/protective agents for the greener synthesis of mNPs with both adsorption properties and enhanced photoactive response in advanced oxidation processes (AOPs) for the remediation of contaminated water (Magnacca et al., 2014).

Polycyclic aromatic hydrocarbons (PAHs) are among the most ubiquitous environmental contaminants (Vane et al., 2013). Due to their resistance to biodegradation and bioaccumulation, the presence of the PAHs in surface water, groundwater, and drinking water, poses a major risk to human health and wildlife. Different techniques have been developed for removing PAHs from contaminated water, among which physical remediation by means of selective adsorbents is one of the most frequently used strategies due to its high effectiveness and low operational cost (Pérez et al., 2008; Dave and Ghaly, 2011).

Conventional adsorbents selected for their high oleophilic properties in contaminated water remediation are polymeric foams in the shape of rolls and/or sheets (typically made of polypropylene, polystyrene, and polyurethane) (Teas et al., 2001; Dave and Ghaly, 2011). Additionally, as reported in the literature, high-surface-area activated carbons and graphitic carbons can be a very interesting alternative as adsorbents in wastewater treatments (Lee et al., 2006; Cesano et al., 2012; Magnacca et al., 2018). Hu et al. (2014) demonstrated the use of compressible carbon nanotube-graphene hybrid aerogels having hydrophobicity and oleophilicity for oil sorption. However, the use of such materials, especially in open-space contaminated areas, presents some limitations, one above all the difficulties in their recovering. Therefore, a step forward in this field is the preparation of easily-recoverable carbon-coated magnet-sensitive materials (Wang et al., 2006; Lu et al., 2007; Hao et al., 2014; Cesano et al., 2016).

Magnetic materials consisting of iron oxides (i.e magnetite/maghemite) particles stabilized by functional carbon shells, received a great attention as easily-recoverable magnet-responsive smart materials for wastewater remediation (Hao et al., 2014; Mehta et al., 2015). Recently, in our previous study (Nisticò et al., 2017), another biowaste-derived substrate (namely, chitosan) was selected as starting material for the preparation of carbon-coated magnet-sensitive composite materials for water remediation from PAHs, with promising results.

Therefore, the aim of this study is the preparation and physicochemical characterization of carbon-coated magnetite/maghemite NPs synthesized through iron salts co-precipitation process in the presence of BBS as initial stabilizers and carbon-source. Pyrolysis under nitrogen atmosphere is carried out at mild condition (550 °C), in order to convert the BBS into a carbon layer without altering the structure and properties of magnetite. Morphology, thermal stability and magnetic properties of such composites mNPs were fully assessed. Adsorption experiments involving the water remediation from a PAHs mixture by direct contact with such BBS-derived carbon-materials and subsequent easily-recovery by magnetic separation are also examined.

2. Material and methods

2.1. Materials

Anhydrous ferric chloride $FeCl_3$ (CAS 7705-08-0, purity $\geq$ 98%, Fluka Chemika) and ferrous sulphate heptahydrate $FeSO_4 \cdot 7H_2O$ (CAS 7782-63-0, purity $\geq$ 99.5%, Fluka Chemika) were selected as iron oxide precursors. Bio-Based Substances (BBS-GC) were obtained following a previously reported procedure (Nisticò et al., 2015) starting from urban composted biowastes (i.e., urban public park trimming and home gardening residues after 180 days of composting) sampled from the process lines of *ACEA Pinerolese Industriale S.p.A.* waste treatment plant in Pinerolo (Italy) in an advanced system that comprises specific technological facilities, developed by *ACEA Pinerolese Industriale S.p.A,* and under European validation. Naphthalene (NAP; $\log K_{ow} = 3.37$), acenaphthene (AC; $\log K_{ow} = 3.98$), acenaphthylene (ACL; $\log K_{ow} = 4.07$), fluorine (FL; $\log K_{ow} = 4.18$), anthracene (ANT; $\log K_{ow} = 4.46$), phenanthrene (PHE; $\log K_{ow} = 4.50$), pyrene (PY; $\log K_{ow} = 4.88$) and fluoranthene (FN; $\log K_{ow} = 4.90$) were purchased from Sigma-Aldrich (purity > 99.0%). The aqueous solutions for adsorption experiments were prepared using ultrapure water Millipore Milli-Q™ and all chemicals were used without further purification.

2.2. Preparation of BBS-derived carbon magnet-sensitive materials

The starting BBS-stabilized magnetite NPs were synthesized following the procedure reported in the literature (Franzoso et al., 2017; Nisticò et al., 2018). In detail, 3.7 g of $FeCl_3$ and 4.17 g of $FeSO_4 \cdot 7H_2O$ (molar ratio Fe(III)/Fe(II) = 1.5) were dissolved in 100 mL of deionized water and heated up to 90 °C. Once the temperature was reached, two solutions were added in sequence: a)

10 mL of 25 vol.% ammonium hydroxide, and b) 50 mL of a previously prepared BBS aqueous solution. Three solutions with different content of BBS were employed: 1, 2, and 3 wt.%, respectively. The mixture was mechanically stirred at 90 °C for 30 min and then cooled down to room temperature (RT). Such dispersions of BBS-stabilized magnetite NPs were purified by washing twice with deionized water, deposited onto glass Petri dishes, and oven-dried at 80 °C overnight. BBS-derived magnetic-materials were then thermally treated in a quartz tube under nitrogen atmosphere (N_2 flux of 250 mL min^{-1}) for 1 h at 550 °C (from RT to the target temperature, heating ramp 5 °C min^{-1}). The resulting materials were manually crumbled in a mortar for the further experiments. In analogy to our previous work (Franzoso et al., 2017), depending on the different BBS amount (1, 2 and 3 wt.%), the obtained NPs were coded with the acronym MB1, MB2 and MB3, respectively. Thermally-treated samples were further coded with pyT, where py stands for pyrolysis, and T refers to the temperature of pyrolysis (550 °C). Magnetite (M0), as obtained following the co-precipitation procedure without the BBS addition, was taken as a neat magnetite/maghemite reference.

2.3. Physicochemical characterization

Scanning electron microscopy (SEM) analyses were carried out by using a ZEISS EVO 50 XVP microscope with LaB_6 source, equipped with detectors for secondary electron collection and energy dispersive X-ray Spectroscopy (EDS). SEM micrographs were obtained after sputtering samples with a 10–15 nm thick gold film. Atomic force microscopy (AFM) and magnetic force microscopy (MFM) measurements were performed by using a modified Nanosurf Easyscan2 AFM instrument, equipped with a 10 μm scan-head, high performance anti-vibration platform in an acoustically insulated enclosure and Faraday cage. AFM and MFM images were obtained in a dual-pass mode: the first scan was for the morphological imaging in the intermittent contact mode, while the second scan was operated at constant-height (H) above the same surface with a magnetic probe (Multi75M-G, Budget Sensors; resonant frequency = 75 kHz, force constant = 3 N m^{-1}) having a tip radius of about 60 nm by monitoring the shifting of the phase and of the amplitude signals. The magnetic tip was magnetized by an external magnet (magnetization along the tip-axis) and tested on a magnetic grid prior to measurements. Magnetization measurements were carried out performing experiments in a LakeShore 7404 vibrating sample magnetometer. The hysteresis loop of the samples was registered at RT cycling the magnetic field from −20000 to 20,000 Oe. X-ray diffraction (XRD) patterns were obtained by using an X'Pert PRO MPD diffractometer from PANalytical, equipped with Cu anode, working at 40 kV and 30 mA, with a Bragg-Brentano geometry, in a flat sample-holder. The acquisition was performed in a 0.02° interval steps, with 45 s $step^{-1}$. Fourier transform infrared (FTIR) spectra were registered in transmission mode using a Bruker Vector 22 spectrophotometer equipped with Globar source, DTGS detector, and working with 128 scans at 4 cm^{-1} resolution in the 4000-400 cm^{-1} range. Samples were analyzed as self-supporting pellets by dispersing the mNPs in KBr (1:20 wt ratio).

2.4. Adsorption experiments

2.4.1. Single component PAH system

Preliminary adsorption experiments were performed using ANT as reference PAH substrate. Kinetic experiments were carried out contacting the adsorbent (500 mg L^{-1}) with an ANT solution (50 μg L^{-1}) at pH 6 and sampling at fixed times up to a maximum of 24 h. After contact, an aliquot of 5 mL was recovered, the solid magnetically separated from the solution and the supernatant analyzed. The effect of BBS amount contained in MB samples on adsorption phenomenon was studied considering [ANT] = 40 μg L^{-1}, [MBpy550] = 20 mg L^{-1}, Contact time = 3 h. The ANT concentration effects on adsorption were studied at three different adsorbent dosage (10 mg L^{-1}, 20 mg L^{-1} and 50 mg L^{-1}). A series of Pyrex-flasks were filled with 100 mL of ANT solutions (40–120 μg L^{-1}) and MB3py550 adsorbent were added under continuous stirring. The flasks were capped and shaken in darkness during 3 h. After contact, an aliquot of 5 mL was recovered, the mNPs magnetically separated from the solution and the supernatant analyzed by fluorescence spectroscopy. All adsorption experiments were carried out in triplicate at 20 ± 1 °C. ANT concentrations were determined by fluorescence measurements obtained by means of a Hitachi F-7000 fluorescence spectrometer. The excitation wavelength selected was 250 nm, slit widths of excitation and emission were 2.5 nm, and 1 cm path length quartz cuvettes were used.

2.4.2. Mixture of PAHs

Adsorption experiments with a mixture of eight PAHs (NAP, ACL, AC, FL, PHE, ANT, FN and PY) on MB3py550 were performed. PAHs mixture solution was prepared from a dilution of PAHs mixture stock solution (20 mg L^{-1} of each PAH in methanol) with ultrapure water and agitation during 48 h at RT in amber borosilicate glass containers. Final methanol concentrations were kept under 0.1% of the total solution volume to avoid co-solvent effects. The initial concentrations of each PAH ranged from 2.2 to 44 μg L^{-1}. Concentrations of each PAH after 24 h of contact with the adsorbent (50 mg L^{-1} of MB3py550) were determined by gas chromatography mass spectrometer (GC–MS) using the following procedure: 200 mL of sample extracted after the magnetic separation was eluted through a Strata RP-18 cartridge; then, PAHs were recovered with 6 mL of dichloromethane. The fraction was concentrated to 1 mL under a nitrogen stream, transferred to a glass vial, and quantitated by GC–MS. A 30 m HP-5 MS fused silica column (0.25 mm i.d., 0.25 μm film thickness) was used. Column temperature was 38 °C for 1 min; it increased up to 300 °C with ramping at 6 °C min^{-1} and was held 5 min at 300 °C. Samples were run in the electron impact mode at 70 eV and in the selected ion monitoring (SIM) mode with a 4.04 s scan time over a 50–450 amu range resolution. Each compound was recognized by a target ion and two qualifiers.

2.4.3. Water-soluble fraction of light crude oil dissolved in freshwater (WSF)

Adsorption experiment with crude oil dissolved in water was performed in order to evaluate the adsorption capacity of the MB3py550 toward a real complex matrix. Light crude oil, obtained from Rincon de los Sauces, Neuquen, Argentina, stored at 4 °C, was used to prepare the WSF. A solution composed of crude oil (300 μg mL^{-1} in methanol) and freshwater at a ratio of 1:100 (v/v) was stirred for 72 h at 20 °C in the dark. WSF was separated using the bottom drain and was stored refrigerated at 4 °C for 24 h. In the adsorption experiment, 10 mg of MB3py550 were added to a 200 mL WSF sample and the mixture was placed on a magnetic shaker and allowed to equilibrate for 24 h at 20 °C, in the dark. Then, the 150 mL of supernatant was magnetically separated and spiked with recovery standards (1-chloro-octadecane). Hydrocarbons concentrations in the supernatant, expressed as total petroleum hydrocarbons (TPHs: C6-C35), diesel range (DRO: C10-C25) and residual range (ORO: >C25-C35) was determined by gas chromatography flame ionization detector (CG-FID) following the procedure described below: 150 mL of sample was eluted through Strata RP-18 cartridge using 6 mL of hexane and 3 mL of dichloromethane. The fraction was concentrated to 1 mL under a nitrogen

stream, transferred to a glass vial and quantified by GC-FID. An Agilent (Miami, USA), 6890 gas chromatograph equipped with a ZB–5 fused silica capillary column (30 m × 0.25 mm i.d., 0.25 μm film thickness) and a flame ionization detector (FID) was used. Analyses were conducted in splitless mode using nitrogen as a carrier gas at a flow rate of 2 mL min^{-1}. The column temperature was programmed from 60 °C to 300 °C at a rate of 6 °C min^{-1} and held at 300 °C for 5 min. Quality control and quality assurance protocols to ensure the accuracy and precision of analyses included: employing blanks and reference material and duplicate samples. The average recoveries based on matrix spiked samples were 70–110% and limit of detections are determined to be 13 μg L^{-1} for TPHs and 17 μg L^{-1} for PAH fraction.

2.5. Regeneration and reuse of BBS-derived carbon magnet-sensitive materials

Each cycle of reuse consisted of two stages: sorption and regeneration. For the sorption, 50 mg of MB3py550 was contacted with 100 mL of 80 μgL^{-1} ANT solution during 3 h. After magnetic separation, an aqueous aliquot was withdrawn for the determination of ANT equilibrium concentration and the remained supernatant was discarded. Later, for the regeneration stage, 10 mL of methanol was added to the MB3py550 and the dispersion was shaking for 10 min. The solid was magnetically separated and the regenerated MB3py550 was then reused for subsequent ANT sorption experiments again.

3. Results and discussion

3.1. Morphological and magnetic characterization

Considering the results of the adsorption study reported below, the main part of the characterization studies described in the following concerns the sample showing the best performance in terms of pollutant removal, i.e. MB3py550 and its precursor MB3.

The morphology of the MB3 and MB3py550, are shown in Fig. 1a–d. From the low-resolution SEM images (Fig. 1a,c), it is clear that both samples are in the form of microagglomerates having irregular shape and exposing a complex surface. At higher magnification (Fig. 1b,d), more evident aggregated nanoparticles with sizes in the 20–80 nm range (at the adopted resolution), are illustrated. From Fig. 1b, it can be also noticed that salts or by-products (evidenced in the figure by the white arrow) can be present in the sample after water washing and drying, while a more homogeneous aspect is obtained for the thermally treated samples (Fig. 1d).

Aggregated nanoparticles, 20–50 nm in sizes, are shown in the topography image of AFM/MFM (Fig. 1e). Besides the AFM topography shown in Fig. 1e, the phase shifting of the same region obtained in a second-pass lifted acquisition was operated at different heights (H = 60 nm, 80 nm, 100 nm) by using the same tip probe for analyzing the magnetic interactions and minimizing topographic effects. The intensity of the negative phase shifting, that is typically associated with the attractive interactions between the tip and the sample (dark regions in Fig. 1f–h), was found to depend on the adopted heights: the higher resolution was obtained at H = 60 nm and the magnetic characteristics of the more prominent nanoparticles were found at H = 80 nm, while at higher heights the signal-to-noise ratio is minimized.

To better investigate the magnetic properties, an extensive characterization was performed. The magnetic properties of all samples are reported in Table S2, whereas magnetization curve profiles of both reference magnetite/maghemite and the MB3-series of samples are reported in Fig. S2. In general, all bare samples (not thermally treated) reveal superparamagnetic behaviors, with negligible remanence (M_r) and very low coercitivity (H_c below 10 Oe). As already reported in our previous work (Franzoso et al., 2017), the values of saturation magnetization (M_s) of bare BBS-stabilized NPs were respectively 56 (MB1), 36 (MB2), and 30 (MB3) emu g^{-1}, thus suggesting a different amount of magnetite/maghemite per gram of sample. Moreover, the decrease in terms of M_s for all the BBS-stabilized samples compared to the neat magnetite M0 (64 emu g^{-1}) is mainly due to the presence of the BBS shell, which induces the reduction of the surface magnetic moments (Kim et al., 2003; Sun et al., 2009; Cesano et al., 2015; Bianco Prevot et al., 2017; Franzoso et al., 2017; Nisticò, 2017b).

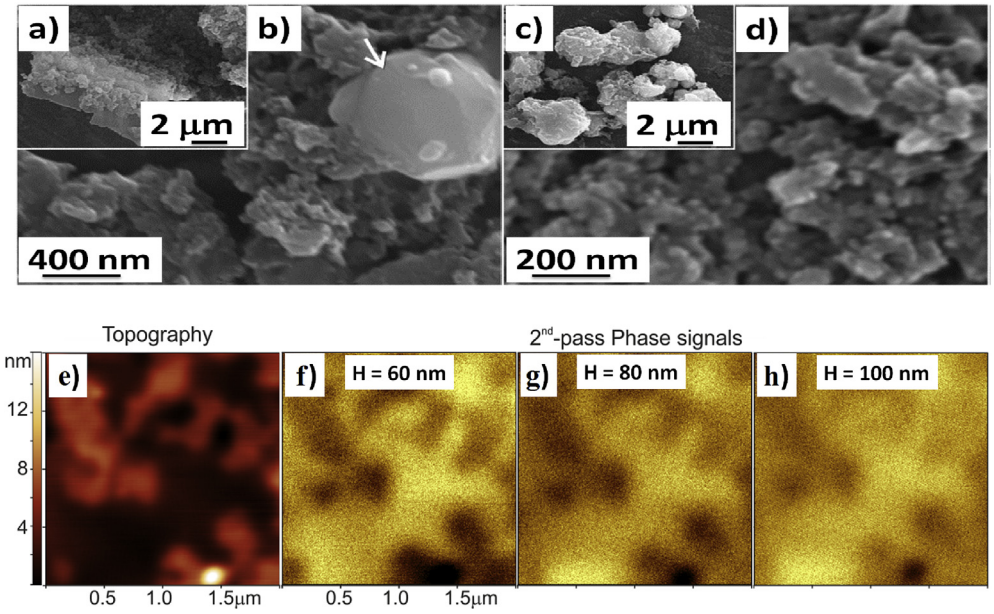

Fig. 1. Low- and high-resolution SEM images of both MB3 (a,b), and MB3py550 (c,d). The arrow in section b) evidences the presence of some synthesis by-product. AFM topography of MB3py550 (e), MFM phase shift images (f,g,h) of region e) obtained at various lift heights (H = 60 nm, 80 nm and 100 nm, respectively).

Conversely, the pyrolysis treatment performed at 550 °C mainly affects the remanence (which moves from almost zero up to 3.4–5.2 emu g^{-1}) and the coercitivity (which increases from less than 10 up to 53–82 Oe). However, saturation magnetization value still remains below the neat magnetite/maghemite M0 value.

3.2. Pyrolysis-induced effects on BBS-derived magnet-sensitive NPs

In order to unveil the chemistry behind the pyrolysis treatments, both XRD and FTIR analyses were performed at different experimental conditions. In particular, the iron oxide phases forming the magnet-responsive inorganic core of the NPs were identified through XRD. For the sake of brevity only the MB3-series of samples are displayed in Fig. 2a.

By considering the bare MB3 sample (Fig. 2a, diffractogram B), all the crystalline planes highlighted in the figure at $2\theta = 30.1°$ (220), 35.4° (311), 43.0° (400), 53.9° (422) 57.2° (511), and 62.6° (440) are consistent with both magnetite (card number 00-019-0629 from ICCD Database) and maghemite (card number 00-039-1346 from ICCD Database) (Cesano et al., 2015). No relevant reflections are expected from BBS since its XRD pattern presents only one broad amorphous contribution centered at ca. $2\theta = 25°$ and few negligible signals due to its ash content (Fig. S3). All the extra signals (not labeled) are consistent with the presence of by-products of the co-precipitation reaction carried out in ammonia aqueous solution, i.e., ammonium-containing salts as ammonium chloride (card number 01-073-0363 from ICCD Database) in analogy to our previous work (Nisticò et al., 2017). Pyrolysis treatments carried out at 550 °C favored the abatement/disappearance of these ammonia-derived salts, maintaining the magnetite/maghemite crystalline phases (Fig. 2a, diffractogram C).

Pyrolysis-induced changes affecting the organic shell and its interaction with the magnetic core of the NPs were followed by means of FTIR analysis in the 4000-500 cm^{-1} range. Infrared spectra of both reference magnetite (M0) and BBS, together with those of the MB3-series are collected in Fig. 2b.

The signals at 575 and 620 cm^{-1} evidenced in M0, MB3 and MB3py500 are due to Fe–O stretching vibrations and consistent with the presence of iron oxides (Fig. 2b, blue box) (Cesano et al., 2015; Franzoso et al., 2017; Nisticò et al., 2017), whereas the presence of BBS in MB3 is confirmed by the presence of the signal at ca. 1600 cm^{-1} due to BBS-carboxylate stretching mode (Bianco Prevot et al., 2017) (Fig. 2b, green box) and 1110 cm^{-1} which can be assigned to C–O stretching vibration. The interaction between BBS and the iron oxide core of the NPs is confirmed by the presence of the very sharp band at 1400 cm^{-1} which is an evidence of the direct interaction between BBS-carboxylate functionalities and the magnetite surface (i.e., carboxylate-iron bond stretching mode) (Ou et al., 2009), and by the shift of the absorption band assigned to C–O stretching mode attributable to the organic matter (mainly polysaccharides and other BBS-derived substances) adsorbed onto the iron oxide surface (Fig. 2b, red box). The thermal treatment carried out at 550 °C (Fig. 2b, curve B) induced the significant reduction of all the infrared signals representative of the BBS-GC coating. On the other hand, the presence of the absorption band at 1620 cm^{-1} typical of the C=C stretching mode, suggesting the incipient conversion of the BBS into graphite-like materials. The iron oxide phase signals at 575 cm^{-1} and 620 cm^{-1} remained unaltered, confirming what already evidenced by XRD results.

These characterization results of MB3py550 and its precursor MB3 were similar to those previously obtained in another synthesis batch (Nisticò et al., 2018), which confirms the reproducibility of the synthesis method.

3.3. Adsorption studies

Fig. 3 shows the kinetic of adsorption of ANT toward both MB3 and MB3py550. The equilibrium was reached after approximately 3 h for MB3py550. Interestingly, MB3 showed some retention capacity toward ANT (70% of removal after 22 h of contact). This could be explained considering that ANT is capable of interacting with the π electrons associated with the aromatic moieties in the BBS matrix. However, a higher ANT % removal was obtained for MB3py550 (ca. 99%), which is expected due to the increased hydrophobicity of the material after pyrolysis and consequent formation of graphite-like structures, thus confirming the results obtained from FTIR spectra. In all cases, pyrolized materials showed higher ANT uptake than non-pyrolyzed materials (data not shown). It is well documented in the literature that π-electron systems of the graphite-like materials can be engaged in π–π electron-donor-acceptor (EDA) interactions with a series of π-donors (e.g., benzene, toluene, PAHs) which can enhance their removal capacity toward aromatic compounds (Zhu and Pignatello, 2005; Keiluweit and Kleber, 2009).

The ANT removal capacity of the three pyrolyzed nanomaterials with different amounts of BBS-GC (i.e. MB1py550, MB2 py550 and MB3 py550) was studied. The best uptake of ANT was observed for MB3py550 (Fig. S4), for this reason this adsorbent was selected for

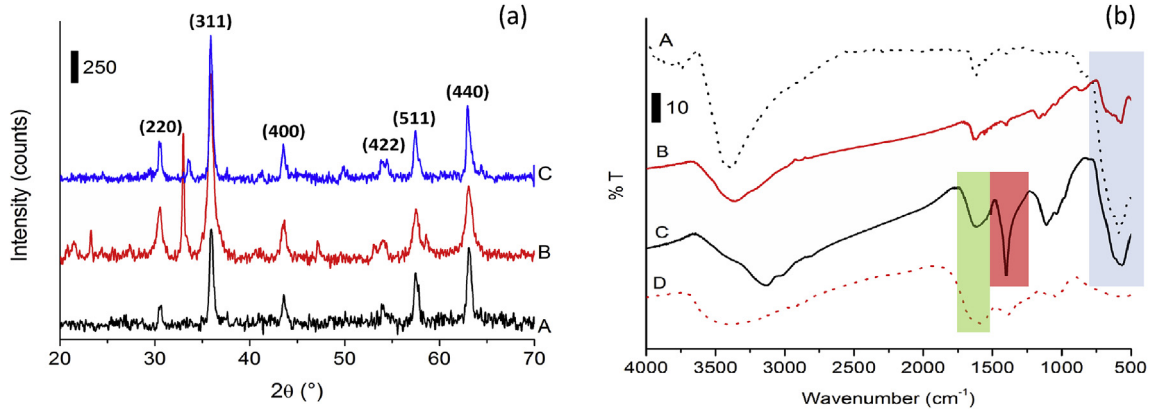

Fig. 2. a. XRD patterns of the neat magnetite M0 (A, solid black curve), MB3 (B, solid red curve), and MB3py550 (C, solid blue curve). Main reflections due to magnetite phase are highlighted. Non-labeled peaks refer to by-products signals. **b.** FTIR spectra in the 4000-500 cm^{-1} range relative to neat magnetite M0 (A, dotted black curve), MB3py550 (B, solid red curve) MB3 (C, solid black curve) and BBS-GC (D, dotted red curve). (For interpretation of the references to colour in this figure legend, the reader is referred to the Web version of this article.)

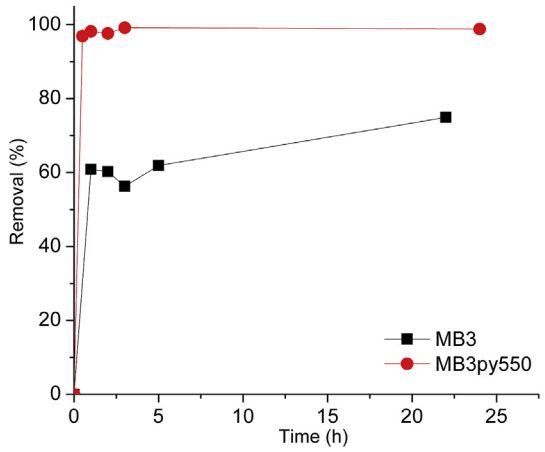

Fig. 3. Kinetics of ANT adsorption on MB3 (black squares, black solid line) and MB3py550 (red circles, red solid line) nanoparticles. [ANT] = 50 μg L^{-1}, [MB3py550] = 500 mg L^{-1}. (For interpretation of the references to colour in this figure legend, the reader is referred to the Web version of this article.)

the investigation of the potential application of these type of materials in different experimental conditions.

In order to optimize the experimental conditions, and in particular to find out the minimum amount of adsorbent needed for an effective ANT removal, sorption experiments were performed by varying the amount of MB3py550 (10, 20 and 50 mg L^{-1}) for different ANT concentration (40, 80 and 120 μg L^{-1}). The ANT removal capacity increased along with the adsorbent amount increase achiving more than 95% removal for all ANT concentration tested with 50 mg L^{-1} of MB3py550 and for 40 μg L^{-1} ANT with 20 mg L^{-1} of adsorbent (Fig. 4).

In order to compare our results with those reported in literature for different nanomaterials, the sorption capacity of ANT, determined as the difference between initial concentration of ANT and the equilibrium concentration of ANT per unit mass of adsorbent, was calculated for each MBSS3py550 dosage and each initial ANT concentration tested in Fig. 4. The highest sorption capacity of ANT on MB3py550 was 4.5 mg g^{-1} corresponding to 20 mg L^{-1} of adsorbent dosage and ANT concentration of 40 μg L^{-1}. In terms of sorption capacity of ANT, MB3py550 is superior to mesostructured silica nanoparticles (1.6 mg g^{-1}) (Topuz and Uyar, 2017), similar to electrospun nanofibrous membranes (4.1 mg g^{-1}) (Dai et al., 2011)

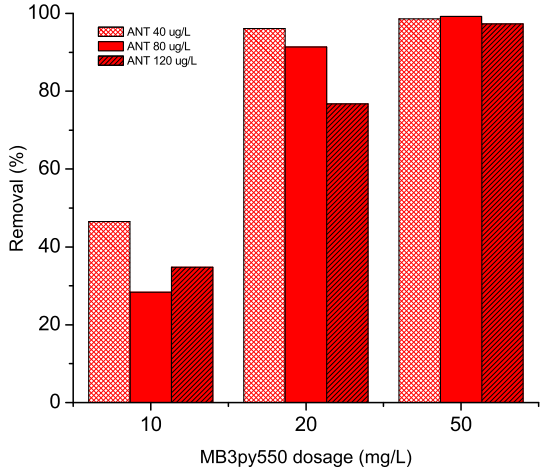

Fig. 4. Effect of initial concentration of ANT and [MB3py550] dosage on ANT removal. Contact time = 3 h. All experiments are performed at both 20 ± 1 °C and pH 6.

and lower than single-walled carbon nanotubes multiwalled carbon nanotubes (Yang et al., 2006). However, being superparamagnetic, the MB3py550 have the unique capability of being magnetically treatable. Moreover, a comparison with previous results obtained with chitosan as a source of carbon for preparing carbon-coated magnetic nanoparticles, shows that MB3py550 have a sorption capacity of ANT almost one order of magnitude higher (Nisticò et al., 2017), which valorizes the use of BBS-GC in this type of sorbents.

To evaluate the removal capacity of MB3py550 towards different PAHs, a mixture of NAP, ACL, AC, FL, PHE, ANT, FN and PY was contacted with 50 mg L^{-1} of adsorbent (Fig. 5a).

The results show different removal capacities depending on the structure of PAHs; in particular, high % removal (>80%) was obtained for FL, ANT, PHE, PY and FN, whereas lower retention was observed for NAP, AC and ACL. The removal capacity increased along with the number of aromatic rings in the polycyclic structure and the PAHs hydrophobicity, suggesting that the pyrolyzed nanomaterials are substantially good in the removal of PAHs from aqueous solutions. Moreover, a clear trend of the removal capacity with the PAHs hydrophobicity (K_{ow}) was also observed (see K_{ow} values in the experimental section). These results can be explained considering that the PAHs sorption occurs following two mechanisms: in the first one the π–π interactions allow the adsorption of the molecules with the more extended aromaticity, whereas in the second one the hydrophobicity of the material attracts PAHs to the adsorbing surface.

Finally, the removal capacity of BBS-derived carbon magnet-sensitive adsorbent toward a sample water spiked with crude oil was studied. The experiment was performed by putting in contact the water-soluble fraction (WSF) with MB3py500 (50 mg L^{-1}) at pH 6 and 20 ± 1 °C. The composition of the WSF used in the experiments was: C12–C25 alkanes (0.78 mg L^{-1}) and C26–C36 alkanes (0.16 mg L^{-1}). It is worth mentioning that the PAHs present in the WSF sample belong to the C26-C36 fraction. Fig. 5b shows a higher uptake of heavier fraction hydrocarbons carried out by MB3py550 (ca. 70% removal), thus meaning that the adsorption capacity increased along with the hydrocarbon hydrophobicity as was also observed for the PAHs adsorption test. These promising results encourage the use of urban wastes as starting materials for the preparation of sustainable substrates to be successfully applied in the removal of hydrocarbons from contaminated waters.

The ANT removal during six continuous cycles of regeneration and reuse are shown in Fig. 6. It was found that no loss of ANT adsorption capacity was observed on the regenerated MB3py550 after six cycles. This reusability of the adsorbent is one of the most important features for their promising applications in environmental detoxification, specifically continuous flow-through systems could be designed for contaminated water treatments with high ANT removal efficiency.

4. Conclusions

Urban composted biowaste-derived substances with a lignin-like structure have proven to be an effective carbon-source for the production of easily-recoverable, low-cost carbon-coated magnet-sensitive NPs, produced through pyrolysis treatments performed in nitrogen at 550 °C. Adsorption experiments testing the removal of PAHs from contaminated water evidenced that the samples thermally treated are effective due to the π-π conjugation between the PAHs and the π-electron system of the pyrolyzed material. The successful adsorption results suggest their possible application in wastewater remediation processes from PAHs-induced pollution.

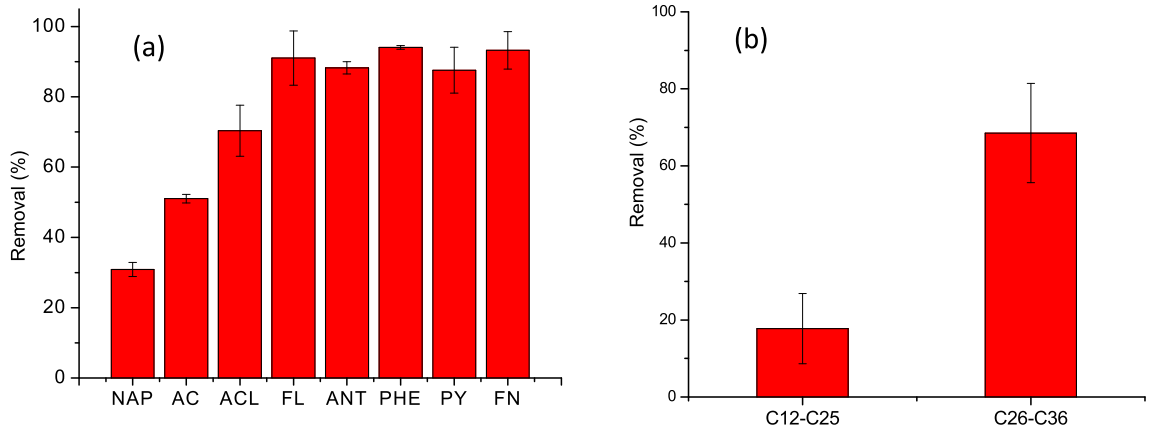

Fig. 5. a. Adsorption experiments of PAHs on MB3py550. [PAHs] = 2.2–44 μg L^{-1}, [MB3py550] = 50 mg L^{-1}, Contact time = 24 h. **b.** Uptake of the water-soluble fraction of crude oil by MB3py550 nanoparticles. Conditions: [TPH] = 0.94 mg L^{-1}, [MB3py550] = 50 mg L^{-1}, Contact time = 24 h. All experiments are performed at 20 ± 1 °C and pH 6. Error bars represent standard deviation of three independent experiments.

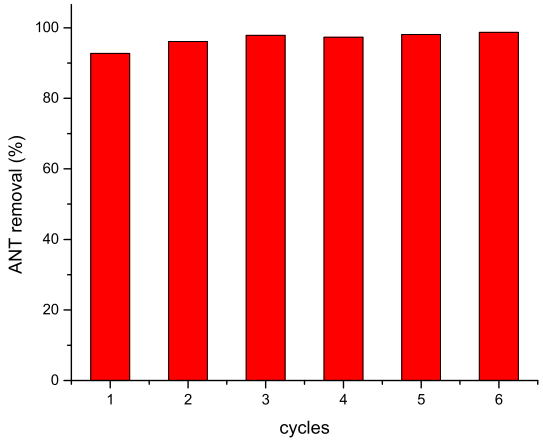

Fig. 6. Cycles of reuse (adsorption shown) of MB3py550 in the removal of ANT. $[ANT]_0$ = 80 μgL^{-1}, [MB3py550] = 500 mgL^{-1}, contact time = 3 h.

Acknowledgements

This work was realized with the financial support for academic interchange by the Marie Sklodowska-Curie Research and Innovation Staff Exchange project funded by the European Commission H2020-MSCA-RISE-2014 within the framework of the research project Mat4treaT (Project number: 645551). Compagnia di San Paolo and University of Torino are gratefully acknowledged for funding Project Torino_call2014_L2_126 through "Bando per il finanziamento di progetti di ricerca di Ateneo – anno 2014" (Project acronym: Microbusters). Polytechnic of Torino is gratefully acknowledged for funding project Starting Grant RTD (project number: 54_RSG17NIR01).The authors are grateful to the Universidad Nacional del Comahue, Argentina, Project 04/I217 for the financial support. Additionally, authors would like to acknowledge Dr. Flavio R. Sives (La Plata, Argentina) for magnetization measurements.

Appendix A. Supplementary data

Supplementary data related to this article can be found at https://doi.org/10.1016/j.chemosphere.2018.03.153.

References

Avetta, P., Nisticò, R., Faga, M.G., D'Angelo, D., Boot, E.A., Lamberti, R., Martorana, S., Calza, P., Fabbri, D., Magnacca, G., 2014. Hernia-repair prosthetic devices functionalised with chitosan and ciprofloxacin coating: controlled release and antibacterial activity. J. Mater. Chem. B 2 (32), 5287–5294.
Bailey, S.E., Olin, T.J., Bricka, R.M., Adrian, D.D., 1999. A review of potentially low-cost sorbents for heavy metals. Water Res. 33 (11), 2469–2479.
Bautista, M.E., Pérez, L., García, M.T., Cuadros, S., Marsal, A., 2015. Valorization of tannery wastes: lipoamino acid surfactant mixtures from the protein fraction of process wastewater. Chem. Eng. J. 262, 399–408.
Bianco Prevot, A., Baino, F., Fabbri, D., Franzoso, F., Magnacca, G., Nisticò, R., Arques, A., 2017. Urban biowaste-derived sensitizing materials for caffeine photodegradation. Environ. Sci. Pollut. R. 24 (14), 12599–12607.
Cesano, F., Fenoglio, G., Carlos, L., Nisticò, R., 2015. One-step synthesis of magnetic chitosan polymer composite films. Appl. Clay Sci. 345, 175–181.
Cesano, F., Rahman, M.M., Bardelli, F., Damin, A., Scarano, D., 2016. Magnetic hybrid carbon via graphitization of polystyrene–co-divinylbenzene: morphology, structure and adsorption properties. ChemistrySelect 1 (10), 2536–2541.
Cesano, F., Rahman, M.M., Bertarione, S., Vitillo, J.G., Scarano, D., Zecchina, A., 2012. Preparation and adsorption properties of activated porous carbons obtained using volatile zinc templating phases. Carbon 50 (5), 2047–2051.
Choi, I.S., Cho, E.J., Moon, J.H., Bae, H.J., 2015a. Onion skin waste as a valorization resource for the by-products quercetin and biosugar. Food Chem. 188, 537–542.
Choi, I.S., Kim, Y.G., Jung, J.K., Bae, H.J., 2015b. Soybean waste (okara) as a valorization biomass for the bioethanol production. Energy 93 (2), 1742–1747.
Dai, Y., Niu, J., Yin, L., Xu, J., Xi, Y., 2011. Sorption of polycyclic aromatic hydrocarbons on electrospun nanofibrous membranes: sorption kinetics and mechanism. J. Hazard Mater. 192 (3), 1409–1417.
Dave, D., Ghaly, A.E., 2011. Remediation technologies for marine oil spills: a critical review and comparative analysis. Am. J. Environ. Sci. 7 (5), 424–440.
Deng, J., You, Y., Sahajwalla, V., Joshi, R.K., 2016. Transforming waste into carbon-based nanomaterials. Carbon 96, 105–115.
Fava, F., Totaro, G., Diels, L., Reis, M., Duarte, J., Carioca, O.B., Poggi-Varaldo, H.M., Ferreira, B.S., 2015. Biowaste biorefinery in Europe: opportunities and research & development needs. N. Biotech. 32 (1), 100–108.
Franzoso, F., Nisticò, R., Cesano, F., Corazzari, I., Turci, F., Scarano, D., Bianco Prevot, A., Magnacca, G., Carlos, L., Mártire, D.O., 2017. Biowaste-derived substances as a tool for obtaining magnet-sensitive materials for environmental applications in wastewater treatments. Chem. Eng. J. 310, 307–316.
Franzoso, F., Vaca-Garcia, C., Rouilly, A., Evon, P., Montoneri, E., Persico, P., Mendichi, R., Nisticò, R., Francavilla, M., 2016. Extruded versus solvent cast blends of poly(vinyl alcohol-co-ethylene) and biopolymers isolated from municipal biowaste. J. Appl. Polym. Sci. 133 (9), 43009.
Hao, W., Björkman, E., Yun, Y., Lilliestr, M., Hedin, N., 2014. Iron oxide nanoparticles embedded in activated carbons prepared from hydrothermally treated waste biomass. ChemSusChem 7 (3), 875–882.
Hu, H., Zhao, Z., Gogotsi, Y., Qiu, J., 2014. Compressible carbon nanotube-graphene hybrid aerogels with superhydrophobicity and superoleophilicity for oil sorption. Environ. Sci. Technol. Lett. 1 (3), 214–220.
Keiluweit, M., Kleber, M., 2009. Molecular-level interactions in soils and sediments: the role of aromatic π-systems. Environ. Sci. Technol. 43 (10), 3421–3429.
Kim, D.K., Mikhaylova, M., Zhang, Y., Muhammed, M., 2003. Protective coating of superparamagnetic iron oxide nanoparticles. Chem. Mater. 15 (8), 1617–1627.
Lata, S., Samadder, S., 2016. Removal of arsenic from water using nano adsorbents and challenges: a review. J. Environ. Sci. 166, 387–406.
Lee, J., Kim, J., Hyeon, T., 2006. Recent progress in the synthesis of porous carbon materials. Adv. Mater. 18 (16), 2073–2094.

Li, Y., Yuan, D., Dong, M., Chai, Z., Fu, G., 2013. Facile and Green synthesis of core-shell structured magnetic chitosan submicrospheres and their surface functionalization. Langmuir 29 (37), 11770–11778.
Lu, A.H., Salabas, E.L., Schüth, F., 2007. Magnetic nanoparticles: synthesis, protection, functionalization, and application. Angew. Chem. Int. Ed. 46 (8), 1222–1244.
Magnacca, G., Allera, A., Montoneri, E., Celi, L., Benito, D.E., Gagliardi, L.G., Gonzalez, M.C., Mártire, D.O., Carlos, L., 2014. Novel magnetite nanoparticles coated with waste-sourced biobased substances as sustainable and renewable adsorbing materials. ACS Sustain. Chem. Eng. 2 (6), 1518–1524.
Magnacca, G., Laurenti, E., Gonzalez, M.C., Arques, A., Prevot, A.B., 2015. Effect of humic substances and bioorganic substrates from urban wastes in nano-structured materials applications and synthesis. In: Arques, A., Prevot, A.B. (Eds.), Soluble Bio-based Substances Isolated from Urban Wastes. Environmental Applications. Springer International Publishing AG, Cham (Switzerland), pp. 41–58.
Magnacca, G., Guerretta, F., Vizintin, A., Benzi, P., Valsania, M.C., Nisticò, R., 2018. Preparation, characterization and environmental/electrochemical energy storage testing of low-cost biochar from natural chitin obtained via pyrolysis at mild conditions. Appl. Surf. Sci. 427, 883–893.
Manna, L., Bugnone, C.A., Banchero, M., 2015. Valorization of hazelnut, coffee and grape wastes through supercritical fluid extraction of triglycerides and polyphenols. J. Supercrit. Fluids 104, 204–211.
Mehta, D., Mazumdar, S., Singh, S.K., 2015. Magnetic adsorbents for the treatment of water/wastewater-A review. J. Water Process Eng 7, 244–265.
Nardi, T., Sangermano, M., Leterrier, Y., Allia, P., Tiberto, P., Månson, J.A.E., 2013. UV-cured transparent magnetic polymer nanocomposites. Polymer 54 (17), 4472–4479.
Nisticò, R., 2017a. Aquatic-derived biomaterials for a sustainable future: a European opportunity. Resources 6, 65.
Nisticò, R., 2017b. Magnetic materials and water treatments for a sustainable future. Res. Chem. Intermed. 3, 6911–6949.
Nisticò, R., Barrasso, M., CarrilloLeRoux, G.A., Seckler, M.M., Sousa, W., Malandrino, M., Magnacca, G., 2015. Biopolymers from composted biowaste as stabilizers for the synthesis of spherical and homogeneously sized silver nanoparticles for textile applications on natural fibers. ChemPhysChem 16, 3902–3909.
Nisticò, R., Franzoso, F., Cesano, F., Scarano, D., Magnacca, G., Parolo, M.E., Carlos, L., 2017. Chitosan-derived iron oxide systems for magnetically guided and efficient water purification processes from polycyclic aromatic hydrocarbons. ACS Sustain. Chem. Eng. 5 (1), 793–801.
Nisticò, R., Celi, L., Prevot, A., Carlos, L., Magnacca, G., Zanzo, E., Martin, M., 2018. Sustainable magnet-responsive nanomaterials for the removal of arsenic from contaminated water. J. Hazard Mater. 342, 260–269.
Ou, X., Chen, S., Quan, X., Zhao, H., 2009. Photochemical activity and characterization of the complex of humic acids with iron(III). J. Geochem. Explor. 102 (2), 49–55.
Pérez, C., Velando, A., Munilla, I., López-Alonso, M., Daniel, O., 2008. Monitoring polycyclic aromatic hydrocarbon pollution in the marine environment after the Prestige oil spill by means of seabird blood analysis. Environ. Sci. Technol. 42 (3), 707–713.
Sun, X., Zheng, C., Zhang, F., Yang, Y., Wu, G., Yu, A., Guan, N., 2009. Size-controlled synthesis of magnetite (Fe_3O_4) nanoparticles coated with glucose and gluconic acid from a single Fe(III) precursor by a sucrose bifunctional hydrothermal method. J. Phys. Chem. C 113 (36), 16002–16008.
Teas, C., Kalligeros, S., Zanikos, F., Stournas, S., Lois, E., Anastopoulos, G., 2001. Investigation of the effectiveness of absorbent materials in oil spills clean up. Desalination 140 (3), 259–264.
Topuz, F., Uyar, T., 2017. Cyclodextrin-functionalized mesostructured silica nanoparticles for removal of polycyclic aromatic hydrocarbons. J. Colloid Interface Sci. 497, 233–241.
Tran, V.S., Ngo, H.H., Guo, W., Zhang, J., Liang, S., Ton-That, C., Zhang, X., 2015. Typical low cost biosorbents for adsorptive removal of specific organic pollutants from water. Bioresour. Technol. 182, 353–363.
Vakili, M., Rafatullah, M., Salamatinia, B., Abdullah, A.Z., Ibrahim, M.H., Tan, K.B., Gholami, Z., Amouzgar, P., 2014. Application of chitosan and its derivatives as adsorbents for dye removal from water and wastewater: a review. Carbohydr. Polym. 113, 115–130.
Vane, C.H., Rawlins, B.G., Kim, A.W., Moss-Hayes, V., Kendrick, C.P., Leng, M.J., 2013. Sedimentary transport and fate of polycyclic aromatic hydrocarbons (PAH) from managed burning of moorland vegetation on a blanket peat, South Yorkshire, UK. Sci. Total Environ. 449, 81–94.
Wang, Z., Guo, H., Yu, Y., He, N., 2006. Synthesis and characterization of a novel magnetic Carrier with its composition of Fe3O4/carbon using hydrothermal reaction. J. Magn. Mater. 302 (2), 397–404.
Yang, K., Zhu, L., Xing, B., 2006. Adsorption of polycyclic aromatic hydrocarbons by carbon nanomaterials. Environ. Sci. Technol. 40 (6), 1855–1861.
Zhao, H., Cui, H.J., Fu, M.L., 2016. A general and facile method for improving carbon coat on magnetic nanoparticles with a thickness control. J. Colloid Interface Sci. 461, 20–24.
Zhu, D., Pignatello, J.J., 2005. Characterization of aromatic compound sorptive interactions with black carbon (Charcoal) assisted by graphite as a model. Environ. Sci. Technol. 39 (7), 2033–2041.